200-years ice core bromine reconstruction at Dome C (Antarctica): observational and modelling results

F. Burgay[1,2], R.P. Fernandez[3], D. Segato[2,4], C. Turetta[2,4], C. S. Blaszczak-Boxe[5], R. H. Rhodes[6], C. Scharchilli[7], V. Ciardini[7], C. Barbante[2,4], A. Saiz-Lopez[8] & A. Spolaor[2,4*]

[1]Paul Scherrer Institute, Laboratory of Environmental Chemistry (LUC), 5232 Villigen PSI, Switzerland

[2]University Ca' Foscari of Venice, Department of Environmental Sciences, Informatics and Statistics, 30172 Venice Mestre, Italy

[3]Institute for Interdisciplinary Science, National Research Council (ICB-CONICET), FCEN-UNCuyo, Mendoza, 5501, Argentina

[4]National Research Council, Institute of Polar Sciences, 30172 Venice Mestre, Italy

[5]Department of Geosciences, The Pennsylvania State University, State College, PA 16803, United States

[6]Department of Earth Sciences, University of Cambridge, Cambridge, United Kingdom

[7]Laboratory of Observations And Measures for the Environment and Climate (SSPT-PROTER-OEM), ENEA, Rome, Italy

[8]Department of Atmospheric Chemistry and Climate, Institute of Physical Chemistry Rocasolano, CSIC, Madrid, Spain

*Corresponding author: andrea.spolaor@unive.it

Keywords (max 6): bromine, ice core, sea-ice variability, Dome C (Antarctica), ozone hole

Key points (max 3)

- Stratospheric ozone-hole depletion has not affected bromine preservation in snow at Dome C
- Volcanic eruptions have not significantly altered the snow bromine profile at Dome C over the last 200 years
- Little seasonal sea-ice variability over the last 30 years and low sensitivity to first-year sea-ice bromine emissions at Dome C do not allow the validation of Br_{enr} as past sea-ice proxy at this site.

1   **Abstract**

2   Bromine enrichment (Br$_{enr}$) has been proposed as an ice core proxy for past sea-ice reconstruction.

3   Understanding the processes that influence bromine preservation in the ice is crucial to achieve a

4   reliable interpretation of ice core signals and to potentially relate them to past sea-ice variability. Here,

5   we present a 210 years bromine record that sheds light on the main processes controlling bromine

6   preservation in the snow and ice at Dome C, East Antarctic plateau. Using observations alongside a

7   modelling approach, we demonstrate that the bromine signal is preserved at Dome C and it is not

8   affected by the strong variations in ultraviolet radiation reaching the Antarctic plateau due to the

9   stratospheric ozone hole. Based on this, we investigate whether the Dome C Br$_{enr}$ record can be used as

10   an effective tracer of past Antarctic sea-ice. Due to the limited time window covered by satellite

11   measurements and the low sea-ice variability observed during the last 30 years in East Antarctica, we

12   cannot fully validate Br$_{enr}$ as an effective proxy for past sea-ice reconstructions at Dome C.

13   **1. Introduction**

14   Halogens play an important role in the chemistry and oxidizing capacity of the Earth's atmosphere:

15   they take part in new particle formation processes, promote mercury oxidation, influence the budget of

16   HO$_x$ and NO$_x$ radicals and cause ozone depletion through efficient catalytic cycles (Saiz-Lopez and

17   Von Glasow, 2012; Simpson et al., 2007). Volcanic eruptions (Gutmann et al., 2018) and the ocean

18   (Parrella et al., 2012; Prados-Roman et al., 2015) represent the main natural sources of halogens to the

19   atmosphere, releasing significant amounts of bromine (Br) and iodine (I) (Cuevas et al., 2018; Carpenter

20   et al., 2013). In this work we focus on bromine, which has been shown to dominate halogen emissions

21   and chemistry in the polar atmosphere through the so-called "bromine explosion events" (Pratt et al.,

22   2013; Platt and Lehrer, 1997). These are heterogeneous autocatalytic photochemical reactions, which

23   were first described in the Arctic boundary layer and that cause the bromine-induced ozone depletion

24   events (Fan and Jacob, 1992; Vogt et al., 1996; Foster et al., 2001; Wennberg, 1999; Barrie et al., 1988;

25   Kreher et al., 1997). These autocatalytic multiphase chain reactions require both acidic conditions and

26   sunlight to produce an exponential increase in atmospheric bromine concentration, mainly as gaseous

27 BrO, Br$_2$ and HOBr (Schönhardt et al., 2012; Zhao et al., 2016; Nghiem et al., 2012). In the polar

28 regions, the most favourable substrate (i.e. with a large bromide content) to produce such bromine

29 explosion and ozone depletion events during springtime is the sea-salt aerosol derived from surface

30 blowing snow deposited over first-year sea-ice (FYSI), which is characterized by acidic conditions,

31 higher Br$^-$/Cl$^-$ ratio (Pratt et al., 2013) and higher salinity than the snow deposited over multi-year sea-

32 ice (MYSI) (Frey et al., 2020). Direct observations from two winter cruises in the Weddell Sea

33 (Antarctica) and model simulation, showed that significant bromine losses take place in the aerosol

34 phase, indicating that sea-salt aerosol debromination from salty blowing snow over sea-ice represents a

35 relevant source of gas-phase inorganic bromine to the troposphere (Frey et al., 2020; Parrella et al.,

36 2012; Yang et al., 2005). Note that most inorganic bromine gases present in the atmosphere are highly

37 water-soluble and they suffer wet and dry deposition over the ice sheets (Legrand et al., 2021; Parrella

38 et al., 2012; Fernandez et al., 2019).

39 Especially during the "bromine explosion events", bromine, that shares the same sources as sodium

40 (i.e. sea-salt), is significantly enriched compared to sodium (Na) in the FYSI surfaces, exceeding the

41 bromine-to-sodium mass ratio of seawater (Millero et al., 2008). Being promoted by the presence of

42 FYSI compared to MYSI, this bromine enrichment (Br$_{enr}$, eq 1) has been proposed as a potential tracer

43 for the reconstruction of past FYSI conditions (Spolaor et al., 2016; Maffezzoli et al., 2019; Spolaor et

44 al., 2013b; Vallelonga et al., 2017). Qualitatively, higher Br$_{enr}$ values were linked to larger FYSI extent

45 (Spolaor et al., 2013b). However, many unknowns, mainly related to the source, transport and

46 preservation of bromine within the snowpack, still remain (Maffezzoli et al., 2019). For example, it has

47 been suggested that the anthropogenic-induced acidity increase of the snow deposited over the sea-ice

48 surface can enhance the sea salt debromination rates enhancing the release of reactive bromine from

49 sea-salt aerosols into the atmosphere (Maselli et al., 2017; Sander et al., 2003). Further, bromine can

50 also be re-emitted from the snowpack after deposition and prior to burial. However, the results obtained

51 from previous studies are contradictory and site-specific (Mcconnell et al., 2017; Legrand et al., 2016;

52 Dibb et al., 2010; Spolaor et al., 2019). In Greenland, Dibb et al., (2010) showed that bromine photo-

53 activation was present during spring/summer and highlighted an efficient Br chemical cycling above

the snow. In the Svalbard Archipelago, a high-temporal resolution study designed to investigate the potential photo-emission of bromine from the snowpack (Spolaor et al., 2019) did not highlight any bromine diurnal cycle, suggesting its preservation in snow. In Antarctica, through the investigation of Na and Br fluxes against snow accumulation rate, McConnell et al., (2017) found that bromine re-emission from the Antarctic snowpack is inversely dependent on the accumulation rate. It was shown that the bromine loss from the snowpack was higher (65%) at sites with the lowest accumulation rate (50 kg m^{-2} yr^{-1}), and it decreased to 11% at sites with high annual accumulation rate (300 kg m^{-2} yr^{-1}). Based on these observations, virtually all bromine deposited at Dome C (Antarctica), where the annual snow accumulation is ≈25-28 kg m^{-2} yr^{-1}, would have been re-emitted to the atmosphere prior to burial (Mcconnell et al., 2017; Maffezzoli et al., 2019). These conclusions contrast with previous observations performed at Dome C that reported no significant bromine re-emission from the snowpack (Legrand et al., 2016). An additional process that can affect bromine preservation within the snowpack has been identified in coincidence with the 17.7 ka Mt. Takahe volcanic eruption, when, the combination of an increased surface ultraviolet (UV) radiation, due to stratospheric ozone depletion, and high acidity conditions was associated with a decrease in ice bromine concentration (Mcconnell et al., 2017). To our knowledge, there are no investigations that focused on the effects of the modern UV-radiation changes reaching the Antarctic plateau, due to the ozone-hole formation, on bromine preservation in snow.

To unravel the physicochemical processes that can influence bromine preservation in the snow, we investigated the main pathways that can induce its emission from the snowpack to the atmosphere. Bromine is mainly present in the Antarctic snowpack as bromide (Spolaor et al., 2013a) and it can be oxidized by OH radicals (George and Anastasio, 2007; Abbatt et al., 2010) to form evaporable gaseous bromine. The main $^\bullet$OH source within the snowpack is the photolysis of hydrogen peroxide (Chu and Anastasio, 2005), nitrate (Chu and Anastasio, 2003; Abbatt et al., 2010) and nitrite (Chu and Anastasio, 2007). Understanding the relevance of each of these photochemical pathways in explaining the preservation of bromide in the Antarctic snowpack before and after the onset of the modern-ozone hole is then crucial for a reliable interpretation of the bromine enrichment profile observed in ice core records.

81   In this study, we present the first bromine record retrieved from a shallow firn core collected at

82   Dome C, Antarctica, covering the period 1800-2012. Through the evaluation of the bromine profile, it

83   is possible to provide new evidence about the role of the enhanced solar-UV radiation due to the onset

84   of the modern Antarctic ozone hole (1975) on bromine preservation in the snowpack. An extended

85   evaluation of the role of $^{\bullet}$OH precursors and their relevance at Dome C is also performed. Lastly, an

86   assessment of the suitability of Br_{enr} as a potential past sea-ice tracer at Dome C is also addressed by

87   combining air-mass transport re-analysis and sea-ice extent satellite observations. The results presented

88   in this paper open new perspectives on future long-term bromine studies from ice cores retrieved from

89   low accumulation areas, aimed at forecasting future deep core drillings at Dome C, such as those

90   planned for the Beyond EPICA project.

91   **2. Material and Methods**

92   *2.1 Ice core sampling and location*

93

94   A 13.72 m shallow ice-core was drilled close to Concordia Station, at Dome C (3233 m a.s.l.;

95   75°05'59''S, 123°19'56''E) in 2012. The retrieved shallow ice-core covers approximately 212 years,

96   from 1800 to 2012. The ice core dating is described in details by Spolaor et al., (2021), with age

97   uncertainties ranging from 1 year at surface to 5 years at the bottom of the core. Dome C is a suitable

98   Antarctic site for performing photochemical studies related to the preservation of reactive elements and

99   halides within the snowpack (Savarino et al., 2007; Cairns et al., 2021; Song et al., 2018; Spolaor et al.,

100   2018; Spolaor et al., 2021). This location presents a low and rather constant accumulation rate ($25.3 \pm$

101   1.3 kg m^{-2} yr^{-1} from 1816-1998, 28.3 ± 1.3 kg m^{-2} yr^{-1} from 1965-1998; 28 kg m^{-2} yr^{-1} from 2004-2011)

102   (Frezzotti et al., 2005; Frezzotti et al., 2013; Genthon et al., 2016), and it is located about 1000 km away

103   from shorelines, thus not being directly affected by local coastal emissions. Matching these criteria is

104   essential for the evaluation of the effects of modern stratospheric ozone loss due to long-lived ozone

105   depleting substances in the potential bromine release from the snowpack.

106   The shallow ice core was collected using a hand drill (3 inches diameter); the sections were sealed

107   in plastic containers and shipped to the Institute of Polar Sciences of the National Research Council

108   (ISP-CNR) in Venice (Italy). The ice core sections were subsequently sampled at 5 ($\pm$ 1) cm resolution

109   (corresponding to approx. 1 year) using a ceramic knife, rinsed with Ultra Pure Water (UPW, Elga Lab,

110   UK) after each use. Only the central part of the core was collected into 50 mL pre-cleaned polyethylene

111   (PE) vials for subsequent analyses, while the outer 2 cm were removed by scraping with a ceramic

112   knife. The core samples were processed in a class 1000 inorganic clean room under a class 100 laminar-

113   flow bench. Samples were kept at -20°C and under dark conditions until the analysis to avoid any

114   possible photolysis reaction. Since we were only interested in the water-soluble bromine and sodium

115   fractions and to avoid potential halogen loss (Flores et al., 2020), the analyses were conducted on melted

116   and not acidified samples by ICP-SFMS (see 2.2). The sodium record considered in this study had some

117   gaps from 1989 to 1997 (n=12, corresponding to 5% of the total amount of samples) that were filled

118   with Na concentration data retrieved from two snowpits collected in 2013 and 2017, as reported in

119   Spolaor et al., 2021.

120   *2.2 Instrumental analysis and cleaning procedure*

121   Total sodium and bromine concentrations were determined by ICP-SFMS following Spolaor et al.,

122   (2016). Each analytical run started and ended with an Ultra-Pure Water (UPW) cleaning session of 3

123   min to ensure a stable background level throughout the analysis. The external standards that were used

124   to calibrate the analytes were prepared by diluting a 1000 ppm stock IC (ion chromatography) standard

125   solution (TraceCERT® purity grade, Sigma-Aldrich, MO, USA). The standard concentrations ranged

126   between 1 and 200 ng g^{-1} for sodium and 0.05 and 0.200 ng g^{-1} for bromine. As for the samples, the

127   standards were not acidified. Precision and accuracy of the measurements were determined through the

128   multiple reading of selected ice samples and external standards, respectively. The relative standard

129   deviation (RSD %) was low for all the analytes, ranging between 3–4% for sodium and 5-7% for

130   bromine, while accuracy, expressed as the ratio between the observed and the true values, was 105%

131   for sodium and 92% for bromine. The instrumental limit of detection (LoD), calculated as three times

132   the standard deviation of the blank (n = 10), was 1 ng g^{-1} for Na and 0.05 ng g^{-1} for Br. Bromine and

133   sodium concentration values were used to calculate bromine enrichment (Br_{enr}) as:

$$Br_{enr} = \frac{[Br]}{[Na]} \cdot 0.0062 \qquad \text{(eq. 1)}$$

134   where Br and Na are the concentrations obtained from the Dome C record and 0.0062 reflects the

135   bromine-to-sodium mass ratio in seawater (Spolaor et al., 2013b; Millero et al., 2008).

136   All the plastic material used for sample storage and analysis was washed 5 times using UPW and

137   filled with UPW for 1 week. Then, it was rinsed again 5 times with UPW and dried under class-100

138   laminar flow hood before use.

139   *2.3 Back-trajectories calculation, satellite observations and statistical analysis*

140   Backward air mass trajectories that reach the Dome C site (75°05'59''S, 123°19'56''E) were

141   calculated to identify the most likely ocean and sea-ice areas that release bromine species to the

142   atmosphere and that can be transported to the interior of Antarctica. Back-trajectories were obtained

143   from the Hybrid Single-Particle Lagrangian Integrated Trajectory (HYSPLIT) model (Stein et al., 2015)

144   using European Centre for Medium-range Weather Forecasts (ECMWF) ERA5 meteorological

145   reanalysis (Hersbach et al., 2020). ERA5 is available on 37 pressure levels with a regular spatial grid

146   of 0.25° x 0.25° at hourly temporal sampling. However, due to the huge amount of trajectories needed

147   for this study, for computation requirements, we considered ERA5 parameters on a spatial grid of 0.5°

148   x 0.5° every three hours and 24 pressure levels (Becagli et al., 2022). 5 days backward trajectories were

149   calculated every 3 h at 1000, 2000 and 3000 meters above Dome C model terrain height for the period

150   1979 – 2018. Each back trajectory was then projected on the Sea-Ice Concentration field (SIC) and the

151   10-m wind field (still in the ECMWF ERA5 reanalysis), associating each value along the trajectory path

152   with the nearest SIC and wind speed values. The main paths of air masses reaching Dome C were

153   highlighted dividing the southern hemisphere in a regular 1° x 1° mesh and counting the total number

154   of back trajectories points at 5 days, falling in each grid cell (i.e. the hours spent by the air mass in each

155   grid cell). Since bromine species are emitted in the marine boundary layer (MBL) (Sander et al., 2003),

156   source bromine areas were evaluated, selecting only the trajectory where the air mass paths lie within

157   the MBL and over sea-ice and counting the total number of resulting points, where conditions are

158   fulfilled, in each of the 1° x 1° grid cells. The height of MBL was set equal to the 900 hPa Isosurface

159   (Lewis et al., 2004) and a value of SIC > 15% were considered in order to simulate the presence of the

160   sea-ice cover (Becagli et al., 2022). The sea-ice concentrations used in this work are derived from

161 passive-microwave radiometers on NASA's satellites. The data are publicly available at the NASA

162 Earth Science portal (https://earth.gsfc.nasa.gov/) and at the National Snow and Ice Data Center portal

163 (http://nsidc.org). The sea-ice extents (in km^2) are calculated as the hemispheric total as well as five

164 regions in the Southern Ocean (Indian Ocean, Western Pacific, Ross sea, Bellingshausen and Amundsen

165 seas and the Weddell sea).

166 The correlations computed among the different variables of this study (Na, Br, Br_{enr}, sea-ice extent

167 data, SAM index) were performed using a 3-year moving average. This choice takes into account both

168 the dating error of the core ($\approx$ 3 years) and the effects of wind erosion on the age distribution of surface

169 snow that spans over more than a year (Picard et al., 2019). To identify any abrupt change point in the

170 records, the *findchangepts()* Matlab (Mathworks) function was used.

171 *2.4 CAM-CHEM model set-up*

172 The wavelength-dependent solar ultraviolet (UV) radiation reaching the Antarctic plateau

173 surface at Dome-C during the 1950-2010 period was computed using the Community Earth System

174 Model (CESM) (Tilmes et al., 2016). The setup of the atmospheric component of the model (CAM-

175 Chem, version 4) was identical to the one used in previous studies addressing the evolution of iodine

176 ice core records in the Arctic (Cuevas et al., 2018) and Antarctica (Spolaor et al., 2021), and considers

177 prescribed sea surface temperatures and sea-ice distributions following the CCMI-REFC1

178 recommendation (Eyring et al., 2013). The CAM-Chem VSL setup includes geographically distributed

179 and seasonally–dependent natural oceanic emissions of five bromocarbons (VSL^{Br} = $CHBr_3$, CH_2Br_2,

180 CH_2BrCl, $CHBrCl_2$, $CHBr_2Cl$) and four iodocarbons (VSL^I = CH_3I, CH_2ICl, CH_2IBr, CH_2I_2), whose

181 oceanic flux is assumed to remain constant during the whole modelling period (Ordóñez et al., 2012).

182 The chemical scheme includes the additional inorganic chlorine and bromine contribution arising from

183 the so-called sea-salt dehalogenation recycling occurring in the marine boundary layer and the free

184 troposphere (Fernandez et al., 2014; Fernandez et al., 2021). The model was configured in free-running

185 mode, with 26 vertical levels expanding from the Earth's surface to approximately 40 km (3.5 hPa in

186 the upper stratosphere), and with a spatial resolution of 1.9º latitude by 2.5º longitude. The CAM-Chem

187 REFC1 configuration used here provides a reasonable representation of the evolution of the size and

188 depth of the ozone hole, presenting an excellent agreement with satellite ozone observations during the

189 modelled period (Fernandez et al., 2017; Spolaor et al., 2021).

190 Here, we compute the photolysis rate constant (J-value) of different $^{\bullet}$OH precursors involved in the

191 preservation of bromine in the snowpack following the same approach used in Spolaor et al., (2021).

192 The molar absorptivities, quantum yields and species concentrations for hydrogen peroxide, nitrate and

193 nitrite at Dome-C are summarized in Table 1. The modeled actinic flux reaching the Antarctic surface

194 includes 100 bins expanding from 121 nm to 750 nm, with a spectral resolution ranging from less than

195 1 nm in the UV to 50 nm in the visible edge. In particular, the model bandwidth within the 280-400 nm

196 spectral range considered in this work poseess a mean resolution of 4 nm. Thus, the CAM-Chem surface

197 actinic flux for each wavelenght grid was linearly interpolated into a 1 nm bandwidth, and the mean J-

198 value during the whole sunlit period (i.e., from September 1st of a given year to February 28th of next

199 year) was computed offline at the closest gridbox to Dome-C (74.84° S; 122.5°E; model mean altitude

200 of 3300 m a.s.l.). The complete sunlit period (spring + summer) was selected because even when the

201 largest changes in surface actinic flux associated with the ozone hole formation are observed during

202 spring, the UV radiation intensity reaching the Antarctic plateau maximizes during the summer (Spolaor

203 et al., 2021).

204 **3   Results and discussion**

205 *3.1 Sodium, bromine and bromine enrichment profiles from the Dome C shallow core*

206 Air masses arriving at Dome C originate from a vast area that extends over the Eastern Antarctic

207 Ocean, Ross Sea and in minimal percentage from West Antarctica. Back trajectory analyses (Figure 1)

208 confirm that the most likely source areas of bromine and sodium emissions during the 1979-2018 period

209 extend from the Indian Ocean sector (IO, 11%) up to the Ross Sea sector (RS, 21%), with the most

210 likely area being the Western Pacific sector (WP, 45%), with the remaining 17% from Bellingshausen

211 and Amundsen seas (B&AS) sector.

The variability in sodium concentration, a conservative tracer that does not show any post-depositional transformation, is used here to evaluate the marine contribution at Dome C (Caiazzo et al., 2021). Sodium concentrations along the entire record spanned from 12 to 117 ng g^{-1}, with an average value of 40 ± 13 ng g^{-1}. Na profile (Figure 2) shows an increase in concentration from 1800 to 1850, followed by a long-term decreasing trend until 1994. Over the last 18 years of the record, higher sodium concentrations were recorded, suggesting an enhanced transport towards Dome C. Bromine concentration at Dome C ranges from below the LoD (0.05 ng g^{-1}) to 0.41 ng g^{-1}, with an average value of 0.10 ± 0.05 ng g^{-1} along the entire record. A significant bromine increase was detected since 2004 when Br concentration increased from 0.10 ± 0.05 ng g^{-1} (pre-2004) to 0.23 ± 0.09 ng g^{-1} (post-2004). The absence of an abrupt change of the bromine signal at the onset of the ozone hole (1975) indicates that Br is preserved in the snowpack independently on the incoming UV-radiation (see section 3.2). Sodium and bromine did not show any significant correlation (r = 0.06, p-value = 0.20) along the entire record, suggesting different deposition velocities during transport from the coast, with sodium being deposited faster than bromine. Indeed, in the polar atmosphere, sodium is present in the aerosol phase and it is mainly affected by wet deposition processes. It was observed that its concentration decreases significantly with distance from the coast, reaching a rather constant deposition rate at approximately 400 km inland (Vallelonga et al., 2021). Contrarily, bromine exists in both the aerosol and in the gas phase, its atmospheric lifetime is also driven by dry deposition processes, it can experience heterogeneous chemical recycling during transport and its concentration gradually decreases from 100 km to 1000 km inland (Simpson et al., 2005; Vallelonga et al., 2021).

Br$_{enr}$ values ranged between 0.07 and 1.6 with an average value of 0.4 ± 0.3 along the entire record. Contrarily to sodium and bromine, the enrichment did not show any significant increase in the recent part of the record. On the contrary, a significant regime change was detected in 1825, when the Br$_{enr}$ mean value changed from 0.7 ± 0.3 (1800-1825) to 0.4 ± 0.3 (1825-2012). A two-sample t-test strengthened the significant difference between the two periods (p-value < .001). In general, Br$_{enr}$ values were mainly below 1 (i.e. bromine is depleted relative to sodium), which is expected at remote locations like Dome C, since the Br to Na ratio depends on the relative transport times of sea salt aerosol and

239   gaseous bromine compounds in the atmosphere (Spolaor et al., 2013b; Simpson et al., 2007; Vallelonga

240   et al., 2021). Thus, our findings agree with the synthesis of Vallelonga et al. (2021), which show low

241   Br_{enr} values near the coast, a gradual increase at 300-600 km inland and a following decrease to values

242   lower than 1 for all sites located more than 800 km from the coast. The few Br_{enr} values higher than 1

243   may indicate larger FYSI surface from the source areas (Spolaor et al., 2016) or different bromine

244   partitioning between the aerosol and gas phase that depends on the aerosol size and, consequently, on

245   atmospheric resident times (Legrand et al., 2016; Maffezzoli et al., 2019; Vallelonga et al., 2021). In

246   addition, changes in background atmospheric ˙OH and NO_x might have had an impact on the gas-phase

247   bromine partitioning between reservoir and reactive species that might have led to a faster bromine

248   deposition since species like $BrONO_2$ and HOBr have larger and more efficient deposition velocities

249   than reactive species like BrO and Br (Saiz-Lopez and Fernandez, 2016; Fernandez et al., 2019).

250   In Antarctica, few other long-term bromine records exist and they were all collected from coastal

251   sites (Spolaor et al., 2013b; Vallelonga et al., 2017). In contrast to Dome C, these records are more

252   directly influenced by local marine contributions. The shorter atmospheric transport time from the

253   source to the deposition location is reflected by the higher Br_{enr} values observed in these cores

254   (Vallelonga et al., 2017).

255   *3.2 Bromine preservation in the snowpack at Dome C*

256   When reaching the snowpack, UV radiation can rapidly break weak chemical bonds and, due to its

257   high energy, can promote photochemical reactions, especially in the UV-A (320–400 nm) and UV-B

258   (290-320 nm) wavelength bands (Grannas et al., 2007). Due to its low accumulation rate, Dome C is

259   the perfect location for performing UV-photolysis studies on chemical species occurring at the ice and

260   snow surface (Frey et al., 2009; Savarino et al., 2007). The stratospheric ozone layer depletion observed

261   since 1975, has caused an increase in the incoming solar UV radiation over Antarctica at $\lambda < 300$ nm,

262   enhancing, for example, the photochemical iodide oxidation and its subsequent release from the

263   snowpack (Spolaor et al., 2021).

264   As highlighted in section 3.1, no significant changes neither in bromine concentration nor in

265   bromine enrichment have been detected at Dome C since 1975, suggesting that, contrarily to iodine

266   (Spolaor et al., 2021), the ≈10-fold enhanced UV-radiation reaching the Antarctic plateau has not altered

267   bromine preservation within the snowpack (Figure 2). Moreover, laboratory and chamber experiments

268   showed enhanced photochemical oxidation and subsequent release of $I_{2(g)}$ from artificial snow/ice and

269   the snowpack through the formation of a critical I-O$_2$ complex having an absorption band centred at

270   290 nm (Kim et al., 2016). At present, there is no evidence and/or available literature describing a

271   similar Br-O$_2$ complex, and/or any other brominated intermediate product, that leads then to the release

272   of $Br_{(2)(g)}$. In fact, the main inorganic route for bromide oxidation requires radical oxidants (e.g. $^{\bullet}OH$) to

273   drive the redox production of hypobromous acid (BrOH) (Artiglia et al., 2017). This oxidized species

274   can then combine with other reduced halide ions to form molecular halogen compounds that are released

275   into the gas phase (eq. 2-5) (George and Anastasio, 2007):

$$Br^- + {}^{\bullet}OH \rightarrow {}^{\bullet}BrOH^- \tag{2}$$

$$^{\bullet}BrOH^- + Br^- \rightarrow {}^{\bullet}Br_2^- + OH^- \tag{3}$$

$$^{\bullet}Br_2^- + HO_2^{\bullet} \rightarrow Br_2 + HO_2^- \tag{4}$$

$$^{\bullet}Br_2^- + {}^{\bullet}Br_2^- \rightarrow Br_2 + 2Br^- \tag{5}$$

276   Over ice and snow substrates, hydroxyl radicals ($^{\bullet}OH$) can be produced by the photolysis of

277   hydrogen peroxide (H$_2$O$_2$), nitrate (NO$_3^-$) and nitrite (NO$_2^-$) (Chu and Anastasio, 2005; Abbatt et al.,

278   2010; Chu and Anastasio, 2007). Between 290-340 nm wavelengths, H$_2$O$_2$ has a wavelength-dependent

279   molar absorptivity that is 2.5-7.1 times lower than that for NO$_3^-$. Nevertheless, H$_2$O$_2$ has a ≈ 160 times

280   greater quantum yield for $^{\bullet}OH$ production (Table 1) that is insensitive to ionic strength, pH and

281   wavelength (Chu and Anastasio, 2005). Therefore, for a given concentration, H$_2$O$_2$ is a much more

282   effective source of $^{\bullet}OH$ than nitrate. To our knowledge, the only H$_2$O$_2$ concentration value available at

283   Dome C is 2 ng g^{-1}, derived from a sample collected at 3.5 m-depth (Frey et al., 2006). This low value,

284   compared to other locations, is consistent with semi-empirical models that predict a complete hydrogen

285   peroxide loss when the accumulation rate is below ≈ 70 kg m^{-2} yr^{-1} and the annual mean temperature is

286   -50°C (Frey et al., 2006). Considering that Dome C has an annual mean accumulation of ≈25-28 kg m^{-}

287   ^{2} yr^{-1} (Genthon et al., 2016) and an annual mean temperature between -54 and -50°C (Genthon et al.,

288   2021), we assume that the majority of the deposited or *in situ* produced H_2O_2 is rapidly lost to the

289   atmosphere.

290   Alternatively, NO_3^- photolysis (Table 1), occurring at wavelengths of 290-340 nm, with a maximum

291   at 320 nm (Winton et al., 2020), can act as a $^\bullet$OH source following the equations 6-9 (Chu and Anastasio,

292   2005; Abbatt et al., 2010; Boxe, 2005):

$$NO_3^- + h\nu \rightarrow NO_2^- + O^- \tag{6}$$

$$O^- + H_2O \rightarrow {}^\bullet OH + OH^- \tag{7}$$

$$H^+ + NO_2^- \rightarrow HONO \tag{8}$$

$$HONO + h\nu \rightarrow {}^\bullet OH + NO \tag{9}$$

293   The $^\bullet$OH radicals, formed by nitrate photolysis can produce $Br_{2(g)}$ following reactions 2-5. The

294   typical snowpack nitrate profile at Dome C ranges between 22 and 147 ng g^{-1} (Caiazzo et al., 2021;

295   Spolaor et al., 2021) and shows an exponential decay in concentration with depth driven by nitrate UV-

296   photolysis and recycling (Winton et al., 2020; Röthlisberger et al., 2000; Savarino et al., 2007). Due to

297   its higher concentration compared with hydrogen peroxide, nitrate may represent a relevant $^\bullet$OH source

298   at Dome C despite its lower quantum yield for $^\bullet$OH production. The nitrate UV-photolysis, followed by

299    $^\bullet$OH formation and $Br_{2(g)}$ emission, has been reported under laboratory conditions with a significant

300   dependency on the ice pH, with the largest $Br_{2(g)}$ emissions observed at low pH (George and Anastasio,

301   2007).

302   Another source of OH radicals is nitrite (Minero et al., 2007), which can be produced by the

303   dissociation of nitrous acid (HONO) in the condensed phase (eq. 10);

$$HONO \leftrightarrow NO_2^- + H^+ \tag{10}$$

304   or by the direct formation from the minor channel (quantum yield of approximately 0.0011) of nitrate

305   photolysis (eq. 6) (Dubowski et al., 2002).

306   Nitrite displays two major absorption bands peaking at 300 and 354 nm and, through its

307   photolysis, it can produce $^{\bullet}OH$ (eq. 11-12):

$$NO_2^- + h\nu \rightarrow NO + {^{\bullet}O^-} \tag{11}$$

$$^{\bullet}O^- + H_2O \rightarrow {^{\bullet}OH} + OH^- \tag{12}$$

308   The $^{\bullet}OH$ quantum yield from nitrite photo-dissociation depends both on the wavelength (increases

309   with decreasing wavelength) and on temperature (decreases with decreasing temperature). In addition,

310   nitrite has a ≈ 2-fold higher molar absorptivity than nitrate between 280 and 300 nm (Chu and Anastasio,

311   2007) and its $^{\bullet}OH$ quantum yield in ice is equal to 0.020 (at 240 K, $\lambda = 300$), which is 6-fold higher than

312   the one calculated for nitrate (Table 1). Unfortunately, there are no direct measurements of nitrite at

313   Dome C, meaning that its concentration needs to be estimated. Following the approach used by Chu

314   and Anastasio (2007), we assumed that at Dome C the nitrite concentration is similar to the one

315   calculated at the South Pole, which is 0.092 ng g^{-1}. This assumption is based on: a) similar superficial

316   NO_3^- concentrations recorded both at the South Pole (99 ng g^{-1}) and at Dome C (90-147 ng g^{-1}); b) the

317   use of NO_3^- photolysis as the main source for nitrite in the snow (Chu and Anastasio, 2007); and c) the

318   similar total UV-radiation intensities and seasonality reaching both locations.

319   To evaluate the relevance of these processes on the OH radical production in the snow-grains and,

320   consequently their role in promoting $Br_{2(g)}$ emission from the snowpack, we modelled the hydrogen

321   peroxide, nitrate and nitrite photo-activation before (1950-1975) and after the ozone hole formation

322   (post-1975) at Dome C, following the wavelength-dependent CAM-Chem model actinic flux output

323   and the methodology described in Spolaor et al.,2021. Both H_2O_2 and NO_3^- exhibited a small, but

324   significant, enhancement on their surface photolysis (J-value) after the onset of the ozone hole (≈20%

325   increase) due to the higher actinic flux reaching the surface at $\lambda < 300$ nm, where most of the H_2O_2

326   absorption occurs, and to a limited extent also NO_3^- (Figure 3, 4). In contrast, NO_2^- does not show a

327   significant trend on their J-values because both absorption bands maximize at longer wavelengths,

328   within a spectral region that is not directly affected by the formation of the ozone hole (Figure 3,4). It

329   is important to notice that the normalized photolysis ratio between the ozone hole period and the pre-

330   ozone hole period, strongly depends on the wavelength range considered to compute the J-value

331   integration. For example, the ratio between the ozone hole and the pre-ozone hole periods for H_2O_2

332   ranges from a minimum value of 1.2 (280-390 nm) to a maximum value larger than 5 (280-300 nm)

333   (Figure S1). Equivalent results are obtained for the J-nitrate and J-nitrite enhancements (Figure S1),

334   although for these species, with the strongest absorption at longer wavelengths, the upper bandwidth

335   limit used to perform the integration should not be located at values below 310-320 nm, which result in

336   an up to 3-fold increase on the normalized ratio during the pre-ozone hole period. For these reasons,

337   and based on the observed molar absorbivities of each species shown in Figure 3a, our best estimate of

338   the normalized photolysis ratio shown in Figure 4c was computed considering the following

339   wavelengths ranges 280-378 nm for H_2O_2, 295-357.5 nm for NO_3^- and 280-390 nm for NO_2^-.

340   Taking into consideration the NO_3^-, H_2O_2, and NO_2^- concentrations at Dome C and the $^\bullet OH$ quantum

341   yields from their photolysis (Table 1), we observed that the rates of $^\bullet OH$ formation especially from the

342   photolysis of H_2O_2 and NO_3^- slightly increased by a factor 1.1 and 1.09 compared to the pre-ozone hole

343   period, while for nitrite the enhancement was almost negligible (1.01). The average contribution of each

344   of this species in producing OH radicals in the snow was the same both before and after the formation

345   of the ozone hole that is 69% from NO_3^-, 23% from H_2O_2, and 8% from NO_2^-. Specifically, the $^\bullet OH$

346   formation rates during the ozone-hole (pre-ozone hole) period from NO_3^-, H_2O_2 and NO_2^- photolysis

347   are equal to $1.14E^{-13}$ ($1.05E^{-13}$) M s^{-1}, 3.80 E^{-13} ($3.47E^{-13}$) M s^{-1} and $1.2E^{-14}$ ($1.2E^{-14}$) M s^{-1}, respectively

348   (Figure 4b). Those values are calculated by multiplying the mean photolysis rate constant for $^\bullet OH$

349   formation during the ozone-hole (pre-ozone hole) period (i.e. $6.4E^{-8}$ ($5.9E^{-8}$) s^{-1} for NO_3^-, 5.9 E^{-6} ($5.36E^{-7}$) s^{-1} for H_2O_2 and 6.2 E^{-5} ($6.2E^{-6}$) s^{-1} for NO_2^-) by the estimated or real snow-grain concentration (110

351   ng g^{-1} or $1.77E^{-6}$ M, for NO_3^-, 2.2 ng g^{-1}, or $6.47E^{-8}$ M, for H_2O_2 and 0.092 ng g^{-1}, or $2E^{-9}$ M, for NO_2^-).

352   Our results are different from those computed at Neumayer station (Chu and Anastasio, 2007), where

353   the dominant contributor to $^\bullet OH$ production was H_2O_2 ($2.3E^{-11}$ M s^{-1}), followed by NO_3^- ($3.9E10^{-13}$ M

354   s^{-1}) and NO_2^- (1.8 $E10^{-13}$ M s^{-1}). Further, the $^\bullet OH$ production rate at Dome C for H_2O_2 is 2-orders of

355   magnitude lower than at Neumayer station, while it is similar for NO_3^-. The contribution of nitrite at

356   Dome C is one order of magnitude lower than that computed at Neumayer station, where nitrite has

357   been already considered as an insignificant source of $^\bullet OH$ because of its very low estimated

358 concentration (Chu and Anastasio, 2007). Overall, we can conclude that the contribution of H_2O_2, NO_3^-

359 and NO_2^- in forming OH radicals is low at Dome C both before and after the ozone hole period and their

360 change in photolysis is unlikely to have affected bromine preservation within the snowpack. This is in

361 agreement with previous empirical observations (Legrand et al., 2016). We then propose that bromine

362 release into the atmosphere can be favoured only in those locations where high snow acidity (e.g. in

363 correspondence to a volcanic horizon or at coastal sites where biogenic marine emissions can enhance

364 snow acidification) and high concentration of $^\cdot$OH precursors (e.g. H_2O_2) are found.

365   *3.3 The role of volcanic eruptions in bromine preservation at Dome C*

366   Volcanic eruptions are a significant halogen source with the emission of large amounts of HCl, HF

367 and HBr (Pyle and Mather, 2009). In particular, BrO formation through heterogeneous photochemical

368 reactions was detected in a volcanic plume where local O_3 destruction occurred (Von Glasow et al.,

369 2009). However, the role of volcanic eruptions in affecting bromine concentration in ice and snow has

370 been poorly addressed. Studies performed in the European Alps (Legrand et al., 2021) and in the West

371 Antarctic Ice Sheet Divide (Mcconnell et al., 2017), showed opposite results, with recorded bromine

372 increase and depletion in coincidence with volcanic events, respectively. The Dome C shallow core

373 presented in this work covers a period characterized by at least seven inter-hemispherical volcanic

374 eruptions that were identified in other snow-pits and deep cores using both $nssSO_4^{2-}$ and Fe(II) as

375 volcanic proxies (Castellano et al., 2005; Burgay et al., 2021; Gautier et al., 2016): Pinatubo/Cerro

376 Hudson (1991, VEI = 6), Agung (1963, VEI = 5), Krakatua (1886, VEI = 6), Cosiguina (1835, VEI =

377 5), Tambora (1815 = 7) and UE 1809 (1809, VEI $\geq$ 5). VEI stands for Volcanic Explosivity Index, a

378 commonly used quantity to define the magnitude of a volcanic eruption (Newhall and Self, 1982). Its

379 values range from 0 (Hawaiian eruption) to 8 (Ultra-Plinian eruption). In this record, we did not detect

380 any clear fingerprint neither as bromine increase nor as depletion compared to the adjacent periods,

381 suggesting a negligible role of volcanic eruptions in affecting the Br snow chemistry in the inland

382 Antarctic plateau (Figure S2). Nevertheless, we highlight that, due to low snow accumulation and to

383 strong wind erosion, not all the volcanic eruptions listed above might be present in our record. Indeed,

384 a previous investigation that compared the sulphate signal from five ice cores drilled 1 meter apart from

each other at Dome C showed a bulk probability of 30% of missing volcanic events when a single core is used as the site reference (Gautier et al., 2016). Among the volcanic events embraced by our record, only Krakatua, Cosiguina and UE 1809 were observed in all the previously mentioned five replicate cores, giving us confidence that for these eruptions the volcanic fingerprint is present also in our record. However, we acknowledge that a proxy-based volcanic reconstruction is missing for our core and, considering the strong spatial variability observed at Dome C, further and more specific studies are needed to investigate the impact of large inter-hemispherical volcanic eruptions on the preservation of bromine in the snowpack.

3.4 Can Br_{enr} at Dome C be used as proxy for past sea-ice extent?

Having presented evidence to demonstrate the preservation of bromine in the snowpack at Dome C and the absence of a link between our Br signal and the formation of the ozone hole, we now investigate the suitability of Dome C Br_{enr} as a proxy for past sea-ice variability. Previous studies supported the use of Br_{enr} in reconstructing past Antarctic sea-ice extent (Vallelonga et al., 2017; Spolaor et al., 2013b). However, these ice core records were retrieved at coastal sites close to local source areas, where Br_{enr} values where enriched with respect to sea water mass ratio. To the contrary, due to its position, Dome C receives atmospheric signals from a vast area of the East Antarctic sector (Figure 1), which extends from the Indian Ocean to the Ross Sea, potentially giving a reconstruction of past-sea-ice extent over a broader region.

Our 200-year ice core record shows that Br_{enr} has an average value of 0.4 ± 0.3, meaning that it is typically depleted at Dome C. This reflects the differences in Na and Br depositions as a function of the distance from the coast, with resulting Br_{enr} values lower than 1 recorded at sites located more than 800 km far from the coast (Vallelonga et al., 2021). Further, due to the low snow accumulation at this location and to the low concentrations of bromine, Br_{enr} values can be influenced by surface snow removal by wind erosion, changes in meteorological patterns and changes in wind field. For these reasons, and with the current state of knowledge, the presented bromine record should be interpreted with caution.

To understand the driving patterns of the Dome C record and its suitability to reconstruct past sea-ice variability, we compare the Dome C Br_{enr} record with the annual averaged Southern Annular Mode (SAM) Marshall index (Marshall, 2003), satellite observations of FYSI extent from the source areas over the period 1979-2012, and with the Law Dome methanesulphonic acid (MSA_{LD}) profile (Curran et al., 2003) (Table 2). SAM describes the poleward/equatorward movement of the westerly winds that circle Antarctica. When these winds, known as Southern Westerly Winds (SWW), contract towards Antarctica, the SAM is in its positive phase, vice-versa it is in its negative phase. The strength of wind patterns likely influences the amount of sea salt aerosols deposited at Dome C (Crosta et al., 2021), as indicated by the positive correlation of Br and Na with SAM index (0.41 and 0.61, p-value < 0.01, respectively). This is in agreement with recent findings that highlight a prominent northward flow during the SAM negative polarity at Dome C (Kino et al., 2021). We did not observe any correlation between the SAM index and Br_{enr} values.

We find that for the past decades, Br_{enr} at Dome C is mainly influenced by Br deposition, given the positive and significant correlation of Br_{enr} with total Br (r = 0.76, p-value $\leq$ 0.01) and the negative correlation with Na (r =-0.37, p-value $\leq$ 0.01) over the entire record (Table 2). Since gas-phase bromine is emitted in enhanced concentrations (with respect to sea-water ratio) from sea-salt aerosol derived from surface blowing snow deposited over FYSI, the Br_{enr} signal at Dome C is likely to be mainly controlled by emissions and recycling from seasonal sea-ice at the Antarctic coast rather than long-range air mass transport of sea salt aerosols (Spolaor et al., 2013b).

To test this hypothesis, we compared our record with FYSI extent data (Parkinson and Cavalieri, 2012) during the satellite era (1979-2012) over the main source areas defined through back trajectory analysis (Figure 1). As previously stated, the large majority of the back-trajectories that reaches Dome C over the period 1979–2018 originated from the WP sector (see Section 3.1, Figure 1). However, we found significant, but weak, correlations between Br_{enr} and FYSI only with the IO sector (11% of the back-trajectory points satisfying bromine loading condition) and the RS (21%) with r = 0.35 (p-value < 0.1) and r = 0.3 (p-value < 0.1), respectively. In contrast, the closer WP sector does not show any significant correlation with Br_{enr} (Table 2). Given the main source areas from back trajectory analysis

438   are located in the WP (45%, Figure 1), we further investigate this sector by considering the MSA record

439   retrieved from the Law Dome ice core (hereafter MSA_{LD}), located at a coastal site facing the WP

440   (Curran et al., 2003). MSA_{LD} shows a positive and significant correlation with the past sea-ice extent in

441   the WP sector (r = 0.89, p-value ≤ 0.01), but it does not correlate with Dome C Br_{enr}, strengthening the

442   idea that Dome C is influenced by a broader source area than Law Dome. Based on these findings, a

443   possible interpretation is that the IO and RS seasonal sea-ice might have a stronger influence on the

444   Dome C Br_{enr} profile than WP, due to their 211% and 157% average larger FYSI extent than the one

445   recorded in the WP (Figure S3), leading to a larger emission of reactive bromine into the atmosphere.

446   Overall, we found a weak, but significant, correlation between the Br_{enr} record and sea-ice extent in East

447   Antarctica (WP+RS+IO) (r = 0.35, p-value ≤ 0.1). Nevertheless, we need to consider that overall sea-

448   ice extent in East Antarctica has not undergone significant changes over the last three decades, with an

449   *inter*-annual variability of ~20%. Moreover, taking into account the observed Br_{enr} depletion at Dome

450   C and the difficulties in capturing relatively small sea-ice variabilities due to snow remobilization,

451   changes in meteorological patterns and in wind fields (Vallelonga et al., 2021), we hypothesize that sea-

452   ice extent variability observed over the last decades has not been large enough to cause a significant

453   variability in the Br_{enr} signal at Dome C. However, it cannot be ruled out that when longer periods which

454   extend further back in the past are considered (e.g. glacial/interglacial transitions), Br_{enr} variations could

455   be used as a qualitative tracer (i.e. to identify transitions between *large* and *small* FYSI extent) for

456   FYSI variability in East Antarctica.

457   **4. Conclusions**

458   In this manuscript we presented the first long-term ice core record of bromine and bromine

459   enrichment from Dome C (Antarctica). Based on observations and modelling results, we propose that

460   bromine is effectively preserved within the Antarctic plateau snowpack regardless of the intensity of

461   the incoming UV-radiation. Furthermore, we find that the change in surface UV-radiation due to ozone

462   hole formation does not affect the contribution of H_2O_2, NO_3^- and NO_2^- to the production of OH radicals

463   and consequently the dominant OH-driven bromide oxidation channel remains slow. We suggest that

464   neither of these photochemical mechanisms are likely to take place at Dome C, mostly due to the low

465 concentration of H_2O_2 and NO_2^- as well as the low $^{\bullet}OH$ quantum yield from the NO_3^- photolysis. Due

466 to the variety of chemical reactions that can influence bromine preservation within the snowpack, we

467 suggest the inclusion of site-specific studies to assess to what extent bromine is preserved at different

468 specific locations, i.e. through the analysis of $^{\bullet}OH$ precursors (H_2O_2, NO_3^- and NO_2^-).

469 Finally, we provided preliminary insights on the effects of volcanic eruptions on the

470 preservation of bromine in snow at Dome C, where we did not observe any influence on the Br record.

471 However, due to the specific and peculiar environmental conditions at Dome C and to the lack of a

472 proxy-based volcanic eruption reconstruction for this record, our findings are not conclusive and we

473 encourage specific investigations on this topic. We also inquired whether Br_{enr} at Dome C can be used

474 as a sea-ice proxy for the East Antarctic sector. Despite finding weak – but significant - correlations

475 with the Indian Ocean and Ross Sea sectors (which are the ones presenting the largest FYSI extents) it

476 is difficult to validate Br_{enr} as an effective proxy for past sea-ice reconstructions in East Antarctica; this

477 is primarily due to low sea-ice variability observed during the last 30 years. Future investigations at

478 Dome C need to focus on glacial/interglacial transitions to assess whether Br_{enr} at Dome C is somehow

479 related to large-scale variations of sea-ice extensions.

Author contribution

481 **F.B.:** conceptualization, data curation, formal analysis, investigation, methodology, visualisation,

482 writing - original draft preparation – **R.P.F.:** data curation, formal analysis, investigation, methodology,

483 software, visualization, writing – original draft preparation, writing – review & editing – **D.S.:** data

484 curation, formal analysis, methodology, software, visualisation, writing – original draft preparation,

485 writing – review & editing – **C.T.:** data curation, methodology, writing – review & editing – **C.S.B-B**:

486 writing – review & editing – **R.H.R.:**, writing – review & editing – **C.S.:** software, writing – review &

487 editing – **V.C.:** software, writing – review & editing – **C.B.:** funding acquisition, supervision, writing

488 – review & editing – **A.S.L.:** investigation, writing – review & editing – **A.S.:** conceptualization,

489 investigation, resources, supervision, writing – review & editing.

Acknowledgments

491   This publication was generated in the frame of Beyond EPICA. The project has received funding from

492   the European Union's Horizon 2020 research and innovation program under grant agreement No.

493   815384 (Oldest Ice Core) and by the "Programma Nazionale per la Ricerca in Antartide" (PNRA,

494   project number PNRA16_00295). This study is also supported by the bilateral international exchange

495   award Royal Society (UK)-CNR titled: *Antarctic sea-ice history: developing robust ice core proxies*

496   (IEC/R2/202110) awarded to RHR and AS. Logistic support is mainly provided by PNRA and IPEV

497   through the Concordia Station system. We acknowledge Dr. Massimo Frezzotti, for providing us

498   physical snow data from Dome C. This is Beyond EPICA publication number XX.

     Figures and Tables

500   **Figure 1 -** 5-days back-trajectory analysis of air masses arriving at the Dome C site for the period 1979-

501   2018. The back-trajectories are calculated at (a,b) 1000 m, (c,d) 2000 m, (e,f) 3000 m above Dome C

502   model terrain height for the period 1979-2018. Maps are divided into five sectors: Indian Ocean (IO,

503   20°-90°), Western Pacific Ocean (WP, 90°-150°), Ross Sea (RS, 160°-230°) and Bellingshausen &

504   Amundsen seas (B&A, 230°-20°). Panels on the left (a, c, e) represent the sum of the total number of

505   backward trajectory points (i.e. hours) within the fifth and the second days, found in each 1° x 1° grid

506   cell. Panels on the right (b, d, f) represent backward trajectory points (i.e. hours) within the MBL that

507   cross areas with > 15% sea ice concentration at the given point of time. Each contour is normalized

508   from 0 to 100 rescaling with respect to its maximum values and resampled to 0.5° x 0.5° grid mesh in

509   order to increase readability. The gray dashed line represents the median ice edge in September

510   (maximum extent) over the period 1979-2018.

511

512
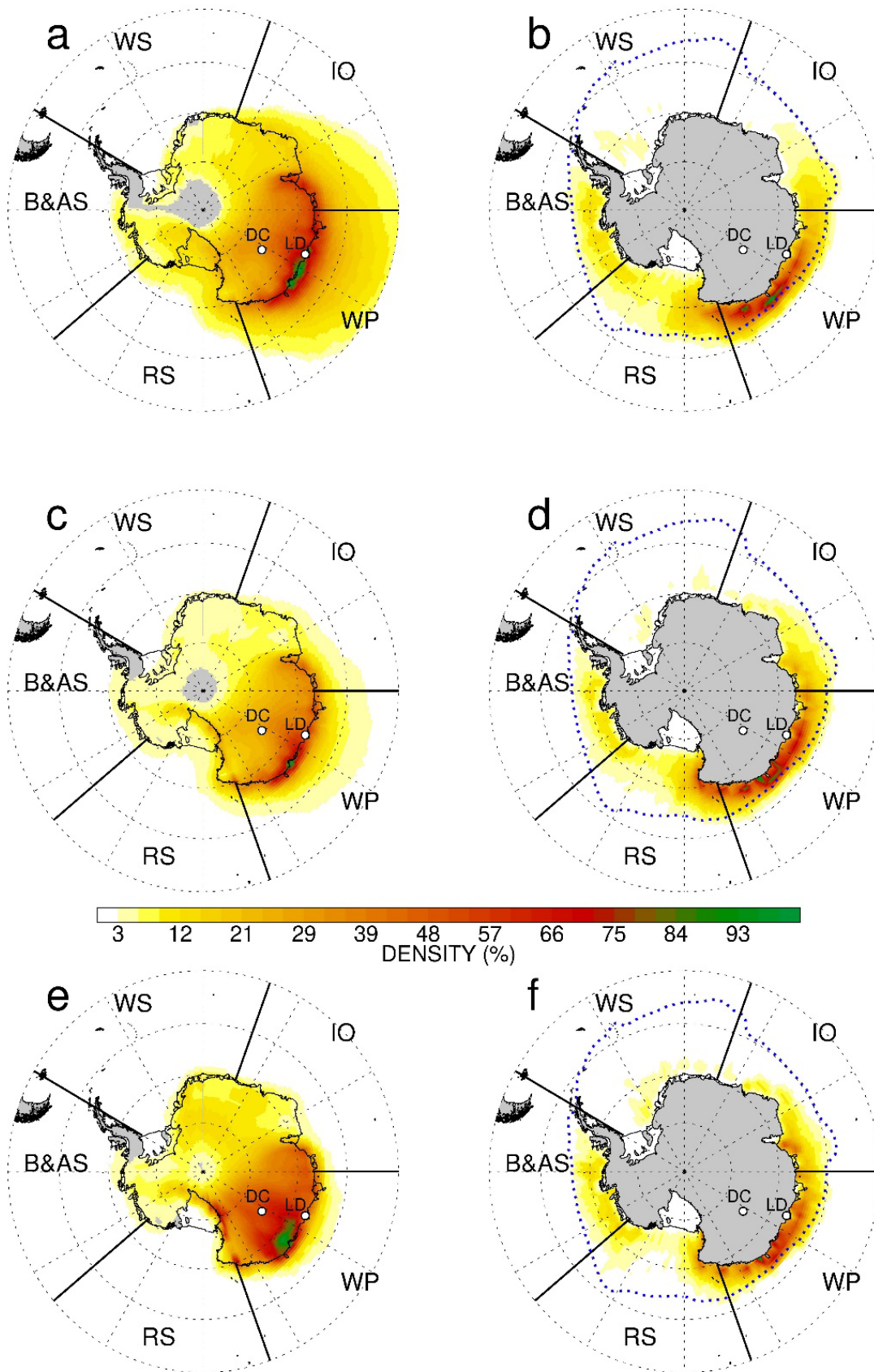
513 **Figure 2** – Sodium (blue line), bromine (red line) and bromine enrichment (yellow line) ice core record

514 from 1800 to 2012. Thick lines refer to a smoothed 3-year moving average.
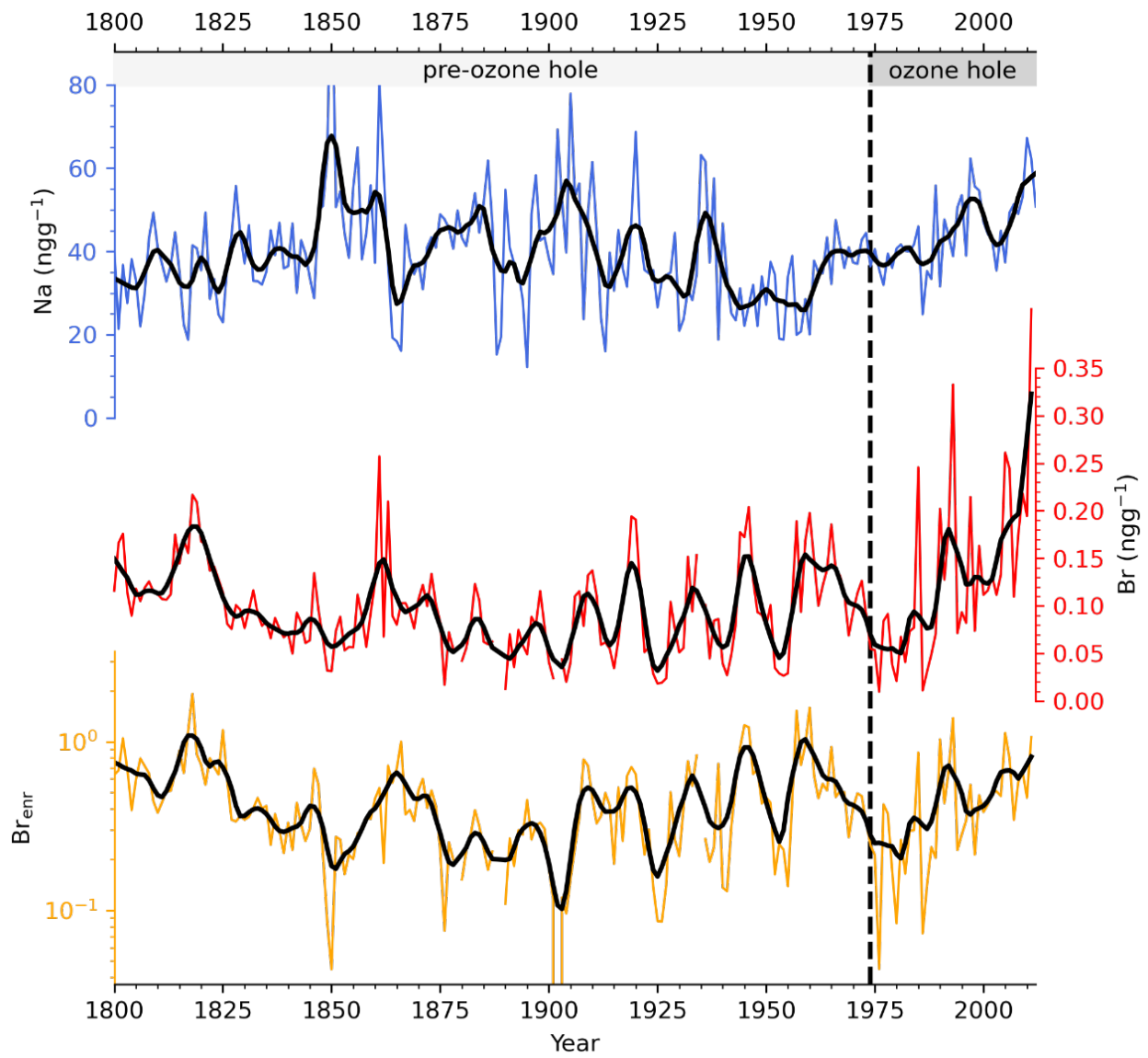
515

516

517

518

519

520

521   **Figure 3** – Panel a), the wavelength dependent actinic flux (AF) at Dome C for different years (coloured

522   dots), superimposed with the absorption spectrum of nitrate (violet line), hydrogen peroxide (orange

523   line) and nitrite (green line). The photolysis rate for the main ˙OH precursors as a function of wavelength

524   in different years (pre and post the modern ozone hole) is shown for panel b) nitrate, panel c) hydrogen

525   peroxide and panel d) nitrite.

526
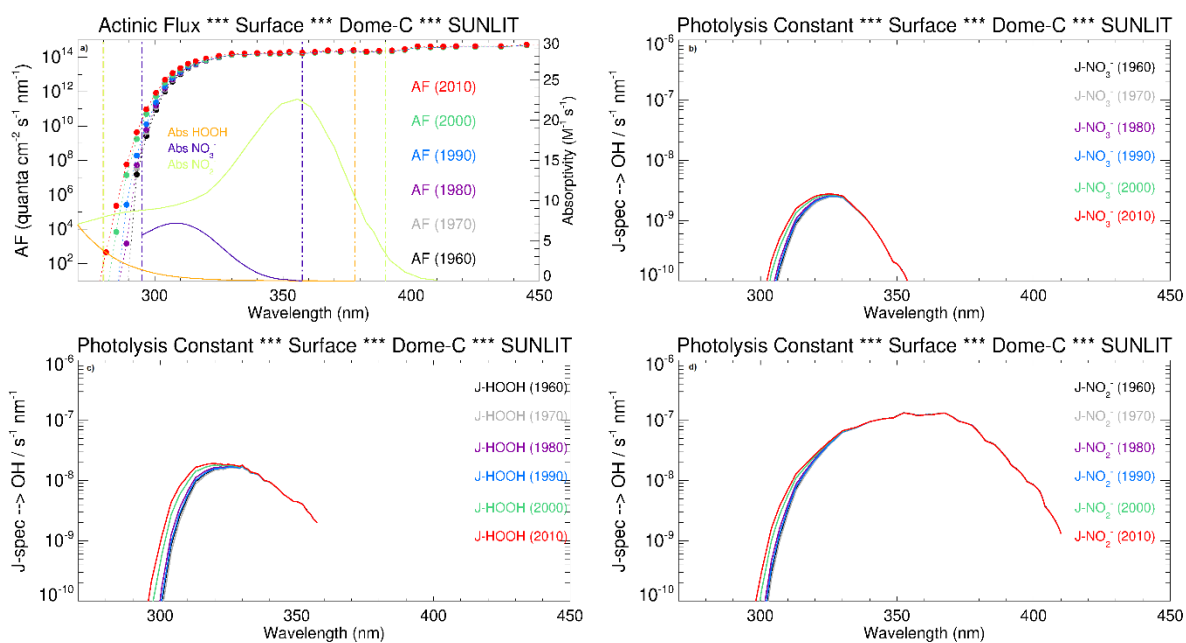
527

528   **Figure 4** – Panel a)**:** the photolysis constant of hydrogen peroxide (orange line), nitrate (violet) and

529   nitrite (green) over the period 1950-2009. Panel b): the ˙OH production rate after the hydrogen peroxide

530   photolysis (orange), nitrate (violet) and nitrite (green) over the period 1950-2009. Panel c): normalized

531   photolysis rate for hydrogen peroxide photolysis (orange line), nitrate (violet line) and nitrite (green

532   line) over the period 1950-2009. The dashed-grey vertical line (1975) represents the beginning of the

533   ozone-hole period. The horizontal-coloured lines represent the average magnitude during the pre-ozone

534   hole period (1950-1975).

535
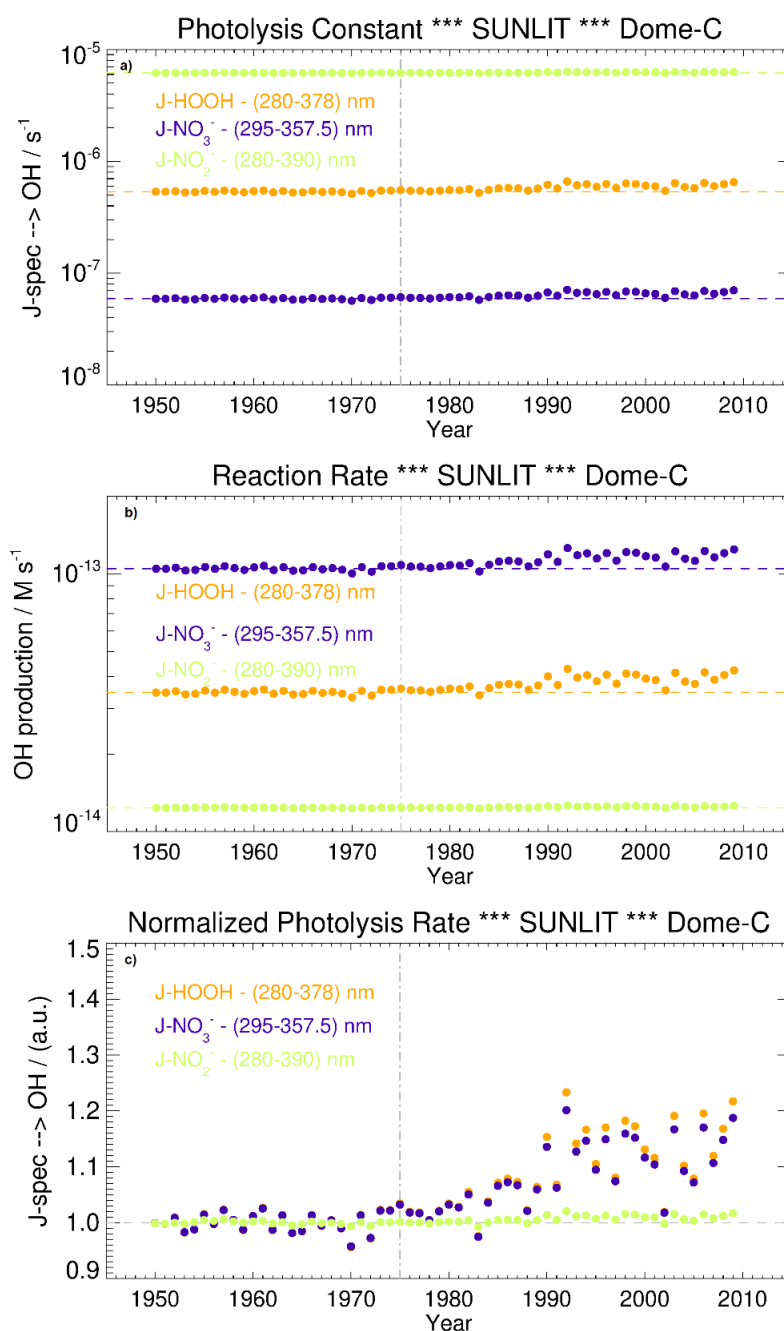
536 **Table 1** – Summary of the ˙OH quantum yields for H_2O_2, NO_3^- and NO_2^-, their molar absorbivities and

537 their concentration at Dome C. *: estimated (more details in the text). [†]: the value is reported from 3.5

538 m depth.

Species	˙OH quantum yield (Chu and Anastasio, 2007, 2005, 2003)	Concentration at Dome C
H_2O_2	0.7	2 ng g^{-1} (Frey et al., 2006)[†]
NO_3^-	0.0034 at pH = 5	110 ng g^{-1} (Spolaor et al., 2021)
NO_2^-	0.020 (T = 260 K, λ = 280 nm)	0.092* ng g^{-1}

539

540

541

542

543 **Table 2** – Pearson correlations of 3-years moving average of Dome C Br, Na and Br$_{enr}$, Law Dome MSA (MSA$_{LD}$) and seasonal sea-ice extents of the Indian

544 Ocean (IO), Western Pacific (WP) and Ross Sea (RS) sectors and of the Eastern Antarctic Ocean (EAO=IO+WP+RS), calculated as $FYSI = \overline{Extent_{Sep-Dec}} -$

545 $Extent_{Feb}$. The moving average is calculated in order to account for a dating error of ~ 3 years. The correlations among the chemical species (Na, Br, Br$_{enr}$ and

546 NO$_3^-$) were made over the entire record (1800-2012), the correlations with MSA$_{LD}$ were done between 1843-1995, the correlations with SAM (Marshall index)

547 were done between 1957-2012, the correlations with sea-ice extents were done between 1979-2012. ***: p-value ≤ 0.01; **: p-value ≤ 0.05; *: p-value ≤ 0.1.

	Na	Br	Br$_{enr}$	NO$_3^-$	MSA$_{LD}$	SAM	IO	WP	RS	EAO
Period		**1800-2012**			**1843-1995**	**1957-2012**		**1979-2012**		
Na	1.0***	0.06	**-0.37***	**0.53***	-0.04	**0.61***	0.16	-0.2	**0.74***	**0.64***
Br	0.06	1.0***	**0.76***	**0.58***	-0.05	**0.41***	**0.36**	-0.24	**0.44**	**0.48***
Br$_{enr}$	**-0.37***	**0.76***	1.0***	**0.45***	0.05	0.18	**0.35*	-0.22	**0.3*	**0.35*
NO$_3^-$	**0.53***	**0.58***	**0.45***	1.0***	0.04	0.24	0.3	-0.23	**0.43**	**0.44**
MSA$_{LD}$	-0.04	-0.05	0.05	0.04	1.0***	-0.08	-0.13	**0.89***	0.32	**0.58**
SAM	**0.61***	**0.41***	0.18	0.24	-0.08	1.0***	0.28	-0.14	**0.58***	**0.58***
IO	0.16	**0.36**	**0.35*	0.3	-0.13	0.28	1.0***	0.0	-0.06	**0.42**
WP	-0.2	-0.24	-0.22	-0.23	**0.89***	-0.14	0	1.0***	-0.03	**0.31*
RS	**0.74***	**0.44**	**0.3*	**0.43**	0.32	**0.58***	-0.06	-0.03	1.0***	**0.82***
EAO	**0.64***	**0.48***	**0.35*	**0.44**	**0.58**	**0.58***	**0.42**	**0.31*	**0.82***	1.0***

548

549   **References**

550   Abbatt, J., Oldridge, N., Symington, A., Chukalovskiy, V., McWhinney, R., Sjostedt, S., and Cox, R.:
551   Release of gas-phase halogens by photolytic generation of OH in frozen halide− nitrate solutions: an
552   active halogen formation mechanism?, The Journal of Physical Chemistry A, 114, 6527-6533, 2010.
553   Artiglia, L., Edebeli, J., Orlando, F., Chen, S., Lee, M.-T., Arroyo, P. C., Gilgen, A., Bartels-Rausch,
554   T., Kleibert, A., and Vazdar, M.: A surface-stabilized ozonide triggers bromide oxidation at the
555   aqueous solution-vapour interface, Nature communications, 8, 1-8, 2017.
556   Barrie, L., Bottenheim, J., Schnell, R., Crutzen, P., and Rasmussen, R.: Ozone destruction and
557   photochemical reactions at polar sunrise in the lower Arctic atmosphere, Nature, 334, 138-141, 1988.
558   Becagli, S., Marchese, C., Caiazzo, L., Ciardini, V., Lazzara, L., Mori, G., Nuccio, C., Scarchilli, C.,
559   Severi, M., and Traversi, R.: Biogenic aerosol in central East Antarctic Plateau as a proxy for the
560   ocean-atmosphere interaction in the Southern Ocean, Science of The Total Environment, 810,
561   151285, 2022.
562   Boxe, C.: Nitrate photochemistry and interrelated chemical phenomena in ice, California Institute of
563   Technology2005.
564   Burgay, F., Barbaro, E., Cappelletti, D., Turetta, C., Gallet, J.-C., Isaksson, E., Stenni, B., Dreossi, G.,
565   Scoto, F., and Barbante, C.: First discrete iron (II) records from Dome C (Antarctica) and the
566   Holtedahlfonna glacier (Svalbard), Chemosphere, 267, 129335, 2021.
567   Caiazzo, L., Becagli, S., Bertinetti, S., Grotti, M., Nava, S., Severi, M., and Traversi, R.: High
568   Resolution Chemical Stratigraphies of Atmospheric Depositions from a 4 m Depth Snow Pit at Dome
569   C (East Antarctica), Atmosphere, 12, 909, 2021.
570   Cairns, W. R., Turetta, C., Maffezzoli, N., Magand, O., Araujo, B. F., Angot, H., Segato, D.,
571   Cristofanelli, P., Sprovieri, F., and Scarchilli, C.: Mercury in precipitated and surface snow at Dome C
572   and a first estimate of mercury depositional fluxes during the Austral summer on the high Antarctic
573   plateau, Atmospheric Environment, 262, 118634, 2021.
574   Carpenter, L. J., MacDonald, S. M., Shaw, M. D., Kumar, R., Saunders, R. W., Parthipan, R., Wilson,
575   J., and Plane, J. M.: Atmospheric iodine levels influenced by sea surface emissions of inorganic
576   iodine, Nature Geoscience, 6, 108-111, 2013.
577   Castellano, E., Becagli, S., Hansson, M., Hutterli, M., Petit, J., Rampino, M., Severi, M., Steffensen,
578   J. P., Traversi, R., and Udisti, R.: Holocene volcanic history as recorded in the sulfate stratigraphy of
579   the European Project for Ice Coring in Antarctica Dome C (EDC96) ice core, Journal of Geophysical
580   Research: Atmospheres, 110, 2005.
581   Chu, L. and Anastasio, C.: Quantum yields of hydroxyl radical and nitrogen dioxide from the
582   photolysis of nitrate on ice, The Journal of Physical Chemistry A, 107, 9594-9602, 2003.
583   Chu, L. and Anastasio, C.: Formation of hydroxyl radical from the photolysis of frozen hydrogen
584   peroxide, The Journal of Physical Chemistry A, 109, 6264-6271, 2005.
585   Chu, L. and Anastasio, C.: Temperature and wavelength dependence of nitrite photolysis in frozen
586   and aqueous solutions, Environmental science & technology, 41, 3626-3632, 2007.
587   Crosta, X., Etourneau, J., Orme, L. C., Dalaiden, Q., Campagne, P., Swingedouw, D., Goosse, H.,
588   Massé, G., Miettinen, A., and McKay, R. M.: Multi-decadal trends in Antarctic sea-ice extent driven
589   by ENSO–SAM over the last 2,000 years, Nature Geoscience, 14, 156-160, 2021.
590   Cuevas, C. A., Maffezzoli, N., Corella, J. P., Spolaor, A., Vallelonga, P., Kjær, H. A., Simonsen, M.,
591   Winstrup, M., Vinther, B., and Horvat, C.: Rapid increase in atmospheric iodine levels in the North
592   Atlantic since the mid-20th century, Nature communications, 9, 1-6, 2018.
593   Curran, M. A., van Ommen, T. D., Morgan, V. I., Phillips, K. L., and Palmer, A. S.: Ice core evidence
594   for Antarctic sea ice decline since the 1950s, Science, 302, 1203-1206, 2003.
595   Dibb, J. E., Ziemba, L. D., Luxford, J., and Beckman, P.: Bromide and other ions in the snow, firn air,
596   and atmospheric boundary layer at Summit during GSHOX, Atmospheric Chemistry and Physics, 10,
597   9931-9942, 2010.
598   Dubowski, Y., Colussi, A., Boxe, C., and Hoffmann, M.: Monotonic increase of nitrite yields in the
599   photolysis of nitrate in ice and water between 238 and 294 K, The Journal of Physical Chemistry A,
600   106, 6967-6971, 2002.

601   Eyring, V., Lamarque, J.-F., Hess, P., Arfeuille, F., Bowman, K., Chipperfiel, M. P., Duncan, B.,
602   Fiore, A., Gettelman, A., and Giorgetta, M. A.: Overview of IGAC/SPARC Chemistry-Climate Model
603   Initiative (CCMI) community simulations in support of upcoming ozone and climate assessments,
604   SPARC newsletter, 40, 48-66, 2013.
605   Fan, S.-M. and Jacob, D. J.: Surface ozone depletion in Arctic spring sustained by bromine reactions
606   on aerosols, Nature, 359, 522-524, 1992.
607   Fernandez, R. P., Kinnison, D. E., Lamarque, J.-F., Tilmes, S., and Saiz-Lopez, A.: Impact of
608   biogenic very short-lived bromine on the Antarctic ozone hole during the 21st century, Atmospheric
609   Chemistry and Physics, 17, 1673-1688, 2017.
610   Fernandez, R. P., Salawitch, R., Kinnison, D., Lamarque, J.-F., and Saiz-Lopez, A.: Bromine
611   partitioning in the tropical tropopause layer: implications for stratospheric injection, Atmospheric
612   Chemistry and Physics, 14, 13391-13410, 2014.
613   Fernandez, R. P., Barrera, J. A., López-Noreña, A. I., Kinnison, D. E., Nicely, J., Salawitch, R. J.,
614   Wales, P. A., Toselli, B. M., Tilmes, S., and Lamarque, J. F.: Intercomparison Between Surrogate,
615   Explicit, and Full Treatments of VSL Bromine Chemistry Within the CAM-Chem Chemistry-Climate
616   Model, Geophysical research letters, 48, e2020GL091125, 2021.
617   Fernandez, R. P., Carmona-Balea, A., Cuevas, C. A., Barrera, J. A., Kinnison, D. E., Lamarque, J. F.,
618   Blaszczak-Boxe, C., Kim, K., Choi, W., and Hay, T.: Modeling the sources and chemistry of polar
619   tropospheric halogens (Cl, Br, and I) using the CAM-Chem Global Chemistry-Climate Model, Journal
620   of Advances in Modeling Earth Systems, 11, 2259-2289, 2019.
621   Flores, E. M., Mello, P. A., Krzyzaniak, S. R., Cauduro, V. H., and Picoloto, R. S.: Challenges and
622   trends for halogen determination by inductively coupled plasma mass spectrometry: a review, Rapid
623   Communications in Mass Spectrometry, 34, e8727, 2020.
624   Foster, K. L., Plastridge, R. A., Bottenheim, J. W., Shepson, P. B., Finlayson-Pitts, B. J., and Spicer,
625   C. W.: The role of Br2 and BrCl in surface ozone destruction at polar sunrise, Science, 291, 471-474,
626   2001.
627   Frey, M. M., Bales, R. C., and McConnell, J. R.: Climate sensitivity of the century-scale hydrogen
628   peroxide (H2O2) record preserved in 23 ice cores from West Antarctica, Journal of Geophysical
629   Research: Atmospheres, 111, 2006.
630   Frey, M. M., Savarino, J., Morin, S., Erbland, J., and Martins, J.: Photolysis imprint in the nitrate
631   stable isotope signal in snow and atmosphere of East Antarctica and implications for reactive nitrogen
632   cycling, Atmospheric Chemistry and Physics, 9, 8681-8696, 2009.
633   Frey, M. M., Norris, S. J., Brooks, I. M., Anderson, P. S., Nishimura, K., Yang, X., Jones, A. E.,
634   Nerentorp Mastromonaco, M. G., Jones, D. H., and Wolff, E. W.: First direct observation of sea salt
635   aerosol production from blowing snow above sea ice, Atmospheric Chemistry and Physics, 20, 2549-
636   2578, 2020.
637   Frezzotti, M., Scarchilli, C., Becagli, S., Proposito, M., and Urbini, S.: A synthesis of the Antarctic
638   surface mass balance during the last 800 yr, The Cryosphere, 7, 303-319, 2013.
639   Frezzotti, M., Pourchet, M., Flora, O., Gandolfi, S., Gay, M., Urbini, S., Vincent, C., Becagli, S.,
640   Gragnani, R., Proposito, M., Severi, M., Traversi, R., Udisti, R., and Fily, M.: Spatial and temporal
641   variability of snow accumulation in East Antarctica from traverse data, J Glaciol, 51, 113-124,
642   10.3189/172756505781829502, 2005.
643   Gautier, E., Savarino, J., Erbland, J., Lanciki, A., and Possenti, P.: Variability of sulfate signal in ice
644   core records based on five replicate cores, Climate of the Past, 12, 103-113, 2016.
645   Genthon, C., Six, D., Scarchilli, C., Ciardini, V., and Frezzotti, M.: Meteorological and snow
646   accumulation gradients across Dome C, East Antarctic plateau, International Journal of Climatology,
647   36, 455-466, 2016.
648   Genthon, C., Veron, D., Vignon, E., Six, D., Dufresne, J.-L., Madeleine, J.-B., Sultan, E., and Forget,
649   F.: 10 years of temperature and wind observation on a 45 m tower at Dome C, East Antarctic plateau,
650   Earth System Science Data, 13, 5731-5746, 2021.
651   George, I. J. and Anastasio, C.: Release of gaseous bromine from the photolysis of nitrate and
652   hydrogen peroxide in simulated sea-salt solutions, Atmospheric Environment, 41, 543-553, 2007.
653   Grannas, A., Jones, A. E., Dibb, J., Ammann, M., Anastasio, C., Beine, H., Bergin, M., Bottenheim,
654   J., Boxe, C., and Carver, G.: An overview of snow photochemistry: evidence, mechanisms and
655   impacts, Atmospheric chemistry and physics, 7, 4329-4373, 2007.

656 Gutmann, A., Bobrowski, N., Roberts, T. J., Rüdiger, J., and Hoffmann, T.: Advances in bromine
657 speciation in volcanic plumes, Frontiers in Earth Science, 6, 213, 2018.
658 Hersbach, H., Bell, B., Berrisford, P., Hirahara, S., Horányi, A., Muñoz-Sabater, J., Nicolas, J.,
659 Peubey, C., Radu, R., and Schepers, D.: The ERA5 global reanalysis, Quarterly Journal of the Royal
660 Meteorological Society, 146, 1999-2049, 2020.
661 Kim, K., Yabushita, A., Okumura, M., Saiz-Lopez, A., Cuevas, C. A., Blaszczak-Boxe, C. S., Min, D.
662 W., Yoon, H.-I., and Choi, W.: Production of molecular iodine and tri-iodide in the frozen solution of
663 iodide: implication for polar atmosphere, Environmental science & technology, 50, 1280-1287, 2016.
664 Kino, K., Okazaki, A., Cauquoin, A., and Yoshimura, K.: Contribution of the Southern Annular Mode
665 to variations in water isotopes of daily precipitation at Dome Fuji, East Antarctica, Journal of
666 Geophysical Research: Atmospheres, 126, e2021JD035397, 2021.
667 Kreher, K., Johnston, P., Wood, S., Nardi, B., and Platt, U.: Ground-based measurements of
668 tropospheric and stratospheric BrO at Arrival Heights, Antarctica, Geophysical Research Letters, 24,
669 3021-3024, 1997.
670 Legrand, M., Yang, X., Preunkert, S., and Theys, N.: Year-round records of sea salt, gaseous, and
671 particulate inorganic bromine in the atmospheric boundary layer at coastal (Dumont d'Urville) and
672 central (Concordia) East Antarctic sites, Journal of geophysical research: atmospheres, 121, 997-1023,
673 2016.
674 Legrand, M., McConnell, J., Preunkert, S., Chellman, N., and Arienzo, M.: Causes of enhanced
675 bromine levels in Alpine ice cores during the 20th century: Implications for bromine in the free
676 European troposphere, Journal of Geophysical Research: Atmospheres, 126, e2020JD034246, 2021.
677 Lewis, E. R., Lewis, R., Lewis, E. R., and Schwartz, S. E.: Sea salt aerosol production: mechanisms,
678 methods, measurements, and models, American geophysical union2004.
679 Maffezzoli, N., Vallelonga, P., Edwards, R., Saiz-Lopez, A., Turetta, C., Kjær, H. A., Barbante, C.,
680 Vinther, B., and Spolaor, A.: A 120 000-year record of sea ice in the North Atlantic?, Climate of the
681 Past, 15, 2031-2051, 2019.
682 Marshall, G. J.: Trends in the Southern Annular Mode from observations and reanalyses, Journal of
683 climate, 16, 4134-4143, 2003.
684 Maselli, O. J., Chellman, N. J., Grieman, M., Layman, L., McConnell, J. R., Pasteris, D., Rhodes, R.
685 H., Saltzman, E., and Sigl, M.: Sea ice and pollution-modulated changes in Greenland ice core
686 methanesulfonate and bromine, Climate of the Past, 13, 39-59, 2017.
687 McConnell, J. R., Burke, A., Dunbar, N. W., Köhler, P., Thomas, J. L., Arienzo, M. M., Chellman, N.
688 J., Maselli, O. J., Sigl, M., and Adkins, J. F.: Synchronous volcanic eruptions and abrupt climate
689 change~ 17.7 ka plausibly linked by stratospheric ozone depletion, Proceedings of the National
690 Academy of Sciences, 114, 10035-10040, 2017.
691 Millero, F. J., Feistel, R., Wright, D. G., and McDougall, T. J.: The composition of Standard Seawater
692 and the definition of the Reference-Composition Salinity Scale, Deep Sea Research Part I:
693 Oceanographic Research Papers, 55, 50-72, 2008.
694 Minero, C., Chiron, S., Falletti, G., Maurino, V., Pelizzetti, E., Ajassa, R., Carlotti, M. E., and Vione,
695 D.: Photochemincal processes involving nitrite in surface water samples, Aquatic Sciences, 69, 71-85,
696 2007.
697 Newhall, C. G. and Self, S.: The volcanic explosivity index (VEI) an estimate of explosive magnitude
698 for historical volcanism, Journal of Geophysical Research: Oceans, 87, 1231-1238, 1982.
699 Nghiem, S. V., Rigor, I. G., Richter, A., Burrows, J. P., Shepson, P. B., Bottenheim, J., Barber, D. G.,
700 Steffen, A., Latonas, J., and Wang, F.: Field and satellite observations of the formation and
701 distribution of Arctic atmospheric bromine above a rejuvenated sea ice cover, Journal of Geophysical
702 Research: Atmospheres, 117, 2012.
703 Ordóñez, C., Lamarque, J.-F., Tilmes, S., Kinnison, D. E., Atlas, E. L., Blake, D. R., Sousa Santos,
704 G., Brasseur, G., and Saiz-Lopez, A.: Bromine and iodine chemistry in a global chemistry-climate
705 model: description and evaluation of very short-lived oceanic sources, Atmospheric Chemistry and
706 Physics, 12, 1423-1447, 2012.
707 Parkinson, C. L. and Cavalieri, D. J.: Antarctic sea ice variability and trends, 1979–2010, The
708 Cryosphere, 6, 871-880, 2012.

709   Parrella, J., Jacob, D. J., Liang, Q., Zhang, Y., Mickley, L. J., Miller, B., Evans, M., Yang, X., Pyle,
710   J., and Theys, N.: Tropospheric bromine chemistry: implications for present and pre-industrial ozone
711   and mercury, Atmospheric Chemistry and Physics, 12, 6723-6740, 2012.
712   Picard, G., Arnaud, L., Caneill, R., Lefebvre, E., and Lamare, M.: Observation of the process of snow
713   accumulation on the Antarctic Plateau by time lapse laser scanning, The Cryosphere, 13, 1983-1999,
714   2019.
715   Platt, U. and Lehrer, E.: ARCTOC Final Report to the European Union, 1997.
716   Prados-Roman, C., Cuevas, C. A., Fernandez, R. P., Kinnison, D. E., Lamarque, J. F., and Saiz-
717   Lopez, A.: A negative feedback between anthropogenic ozone pollution and enhanced ocean
718   emissions of iodine, Atmospheric Chemistry and Physics, 15, 2215-2224, 2015.
719   Pratt, K. A., Custard, K. D., Shepson, P. B., Douglas, T. A., Pöhler, D., General, S., Zielcke, J.,
720   Simpson, W. R., Platt, U., and Tanner, D. J.: Photochemical production of molecular bromine in
721   Arctic surface snowpacks, Nature Geoscience, 6, 351-356, 2013.
722   Pyle, D. and Mather, T.: Halogens in igneous processes and their fluxes to the atmosphere and oceans
723   from volcanic activity: A review, Chemical Geology, 263, 110-121, 2009.
724   Röthlisberger, R., Hutterli, M. A., Sommer, S., Wolff, E. W., and Mulvaney, R.: Factors controlling
725   nitrate in ice cores: Evidence from the Dome C deep ice core, Journal of Geophysical Research:
726   Atmospheres, 105, 20565-20572, 2000.
727   Saiz-Lopez, A. and von Glasow, R.: Reactive halogen chemistry in the troposphere, Chemical Society
728   Reviews, 41, 6448-6472, 2012.
729   Saiz-Lopez, A. and Fernandez, R. P.: On the formation of tropical rings of atomic halogens: Causes
730   and implications, Geophysical Research Letters, 43, 2928-2935, 2016.
731   Sander, R., Keene, W., Pszenny, A., Arimoto, R., Ayers, G., Baboukas, E., Cainey, J., Crutzen, P.,
732   Duce, R., and Hönninger, G.: Inorganic bromine in the marine boundary layer: a critical review,
733   Atmospheric Chemistry and Physics, 3, 1301-1336, 2003.
734   Savarino, J., Kaiser, J., Morin, S., Sigman, D. M., and Thiemens, M.: Nitrogen and oxygen isotopic
735   constraints on the origin of atmospheric nitrate in coastal Antarctica, Atmospheric Chemistry and
736   Physics, 7, 1925-1945, 2007.
737   Schönhardt, A., Begoin, M., Richter, A., Wittrock, F., Kaleschke, L., Gómez Martín, J., and Burrows,
738   J.: Simultaneous satellite observations of IO and BrO over Antarctica, Atmospheric Chemistry and
739   Physics, 12, 6565-6580, 2012.
740   Simpson, W. R., Alvarez-Aviles, L., Douglas, T. A., Sturm, M., and Domine, F.: Halogens in the
741   coastal snow pack near Barrow, Alaska: Evidence for active bromine air-snow chemistry during
742   springtime, Geophysical research letters, 32, 2005.
743   Simpson, W. R., Glasow, R. v., Riedel, K., Anderson, P., Ariya, P., Bottenheim, J., Burrows, J.,
744   Carpenter, L., Frieß, U., and Goodsite, M. E.: Halogens and their role in polar boundary-layer ozone
745   depletion, Atmospheric Chemistry and Physics, 7, 4375-4418, 2007.
746   Song, S., Angot, H., Selin, N. E., Gallée, H., Sprovieri, F., Pirrone, N., Helmig, D., Savarino, J.,
747   Magand, O., and Dommergue, A.: Understanding mercury oxidation and air–snow exchange on the
748   East Antarctic Plateau: a modeling study, Atmospheric Chemistry and Physics, 18, 15825-15840,
749   2018.
750   Spolaor, A., Angot, H., Roman, M., Dommergue, A., Scarchilli, C., Vardè, M., Del Guasta, M.,
751   Pedeli, X., Varin, C., and Sprovieri, F.: Feedback mechanisms between snow and atmospheric
752   mercury: Results and observations from field campaigns on the Antarctic plateau, Chemosphere, 197,
753   306-317, 2018.
754   Spolaor, A., Barbaro, E., Cappelletti, D., Turetta, C., Mazzola, M., Giardi, F., Björkman, M. P.,
755   Lucchetta, F., Dallo, F., and Aspmo Pfaffhuber, K.: Diurnal cycle of iodine, bromine, and mercury
756   concentrations in Svalbard surface snow, 2019.
757   Spolaor, A., Vallelonga, P., Gabrieli, J., Kehrwald, N., Turetta, C., Cozzi, G., Poto, L., Plane, J.,
758   Boutron, C., and Barbante, C.: Speciation analysis of iodine and bromine at picogram-per-gram levels
759   in polar ice, Analytical and bioanalytical chemistry, 405, 647-654, 2013a.
760   Spolaor, A., Vallelonga, P., Plane, J., Kehrwald, N., Gabrieli, J., Varin, C., Turetta, C., Cozzi, G.,
761   Kumar, R., and Boutron, C.: Halogen species record Antarctic sea ice extent over glacial–interglacial
762   periods, Atmospheric Chemistry and Physics, 13, 6623-6635, 2013b.

763   Spolaor, A., Vallelonga, P., Turetta, C., Maffezzoli, N., Cozzi, G., Gabrieli, J., Barbante, C., Goto-
764   Azuma, K., Saiz-Lopez, A., Cuevas, C. A., and Dahl-Jensen, D.: Canadian Arctic sea ice
765   reconstructed from bromine in the Greenland NEEM ice core, Scientific Reports, 6, 33925,
766   10.1038/srep33925, 2016.
767   Spolaor, A., Burgay, F., Fernandez, R. P., Turetta, C., Cuevas, C. A., Kim, K., Kinnison, D. E.,
768   Lamarque, J.-F., de Blasi, F., Barbaro, E., Corella, J. P., Vallelonga, P., Frezzotti, M., Barbante, C.,
769   and Saiz-Lopez, A.: Antarctic ozone hole modifies iodine geochemistry on the Antarctic Plateau,
770   Nature Communications, 12, 5836, 10.1038/s41467-021-26109-x, 2021.
771   Stein, A., Draxler, R. R., Rolph, G. D., Stunder, B. J., Cohen, M., and Ngan, F.: NOAA's HYSPLIT
772   atmospheric transport and dispersion modeling system, Bulletin of the American Meteorological
773   Society, 96, 2059-2077, 2015.
774   Tilmes, S., Lamarque, J.-F., Emmons, L. K., Kinnison, D. E., Marsh, D., Garcia, R. R., Smith, A. K.,
775   Neely, R. R., Conley, A., and Vitt, F.: Representation of the community earth system model (CESM1)
776   CAM4-chem within the chemistry-climate model initiative (CCMI), Geoscientific Model
777   Development, 9, 1853-1890, 2016.
778   Vallelonga, P., Maffezzoli, N., Saiz-Lopez, A., Scoto, F., Kjær, H. A., and Spolaor, A.: Sea-ice
779   reconstructions from bromine and iodine in ice cores, Quaternary Science Reviews, 269, 107133,
780   2021.
781   Vallelonga, P., Maffezzoli, N., Moy, A. D., Curran, M. A., Vance, T. R., Edwards, R., Hughes, G.,
782   Barker, E., Spreen, G., and Saiz-Lopez, A.: Sea-ice-related halogen enrichment at Law Dome, coastal
783   East Antarctica, Climate of the Past, 13, 171-184, 2017.
784   Vogt, R., Crutzen, P. J., and Sander, R.: A mechanism for halogen release from sea-salt aerosol in the
785   remote marine boundary layer, Nature, 383, 327-330, 1996.
786   von Glasow, R., Bobrowski, N., and Kern, C.: The effects of volcanic eruptions on atmospheric
787   chemistry, Chemical Geology, 263, 131-142, 2009.
788   Wennberg, P.: Bromine explosion, Nature, 397, 299-301, 1999.
789   Winton, V. H. L., Ming, A., Caillon, N., Hauge, L., Jones, A. E., Savarino, J., Yang, X., and Frey, M.
790   M.: Deposition, recycling, and archival of nitrate stable isotopes between the air–snow interface:
791   comparison between Dronning Maud Land and Dome C, Antarctica, Atmospheric Chemistry and
792   Physics, 20, 5861-5885, 2020.
793   Yang, X., Cox, R. A., Warwick, N. J., Pyle, J. A., Carver, G. D., O'Connor, F. M., and Savage, N. H.:
794   Tropospheric bromine chemistry and its impacts on ozone: A model study, Journal of Geophysical
795   Research: Atmospheres, 110, 2005.
796   Zhao, X., Strong, K., Adams, C., Schofield, R., Yang, X., Richter, A., Friess, U., Blechschmidt, A.
797   M., and Koo, J. H.: A case study of a transported bromine explosion event in the Canadian high arctic,
798   Journal of Geophysical Research: Atmospheres, 121, 457-477, 2016.

799